Metals & corrosion

Cross-linking and silanization of clay-based multilayer films for improved corrosion protection of steel

Carolyn T. Long[1], Lin Chen[2], Ethan T. Iverson[3], Homero Castaneda[2,*], and Jaime C. Grunlan[1,2,3,*] [iD]

[1] *Department of Mechanical Engineering, TAMU, College Station, TX 77840-3123, USA*
[2] *Department of Materials Science and Engineering, TAMU, College Station, TX 77840-3123, USA*
[3] *Department of Chemistry, TAMU, College Station, TX 77840-3123, USA*

ABSTRACT

The potential for polymer–clay thin film composite coatings to replace environmentally-damaging phosphate conversion coatings on steel is demonstrated. Polyethylenimine and vermiculite clay are used in the layer-by-layer deposition of a 300 nm thick nanobrick wall thin film that hinders the diffusion of corrosive ions. The corrosion prevention performance of the coating is improved through cross-linking with glutaraldehyde and silanization of steel with aminopropyltriethoxysilane prior to film deposition. Finally, the nanobrick wall film is tested with an epoxy topcoat, to demonstrate the viability of the recipe as a primer. Epoxy with the cross-linked and silanized nanobrick wall primer coating outperforms a neat epoxy coating. This unique coating shows tremendous potential for use as an environmentally-benign primer for steel.

GRAPHICAL ABSTRACT
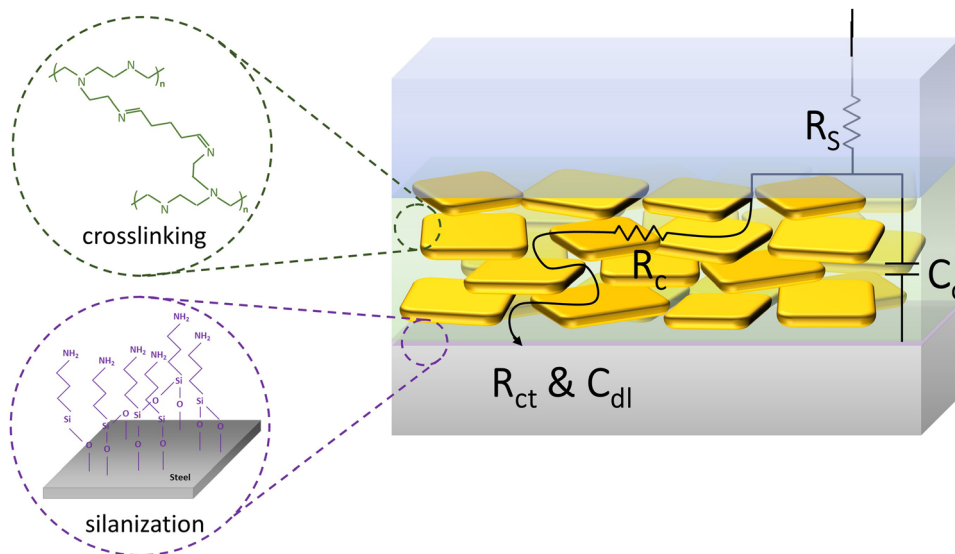
Introduction

A primary drawback to the prevalent utilization of metals is their susceptibility to corrosion, which causes embrittlement [1, 2]. The degradation of metals has led to numerous safety and economic issues [3–5]. Part of this impact stems from the need for excessive, and sometimes redundant, engineering, maintenance, and replacement of materials over time to prevent failure [6]. Corrosion is exacerbated in harsh environments where metals are exposed to salt water, acids, or alkalies. Several strategies, including electrochemical protection, corrosion inhibiting additives, and multilayer insulating coatings, have been developed to prevent or suppress corrosion [7]. Among these strategies, applying multilayer coatings to a metal surface is the most common, consisting of a pretreatment primer layer, several intermediate layers, and a topcoat [8]. For protecting steel, the most effective primer layers are phosphate conversion coatings (i.e., zinc phosphate), which promote corrosion resistance through improved adhesion between a topcoat layer and the steel substrate [9, 10]. Unfortunately, phosphate coatings have been found to be harmful to the environment and human health,

with many municipalities limiting the amount of phosphate that can be discharged into the environment [11]. As a result, environmentally-benign pretreatment coatings have received significant attention. Viable pretreatment layers exhibit both improved adhesion between an intermediate or topcoat and the vulnerable substrate and independent corrosion resistance.

Thin organic–inorganic hybrid films can provide a barrier against corrosive species (i.e., water, oxygen, and aggressive ions) [12, 13]. Inorganic fillers, especially clay nanoplatelets, have attracted attention due to their high in-plane strength and stiffness coupled with their impermeability to various gas species [14–16]. Layer-by-layer (LbL) deposition of polymer–clay nanocomposite thin films generates a nanobrick wall structure [17]. This structure forms a tortuous pathway, hindering the diffusion of small molecule species. The nanobrick wall has proven effective in gas barrier and moisture barrier applications, which makes it a viable candidate as an effective corrosion resistant coating [15, 18, 19]. The present study focuses on improving a LbL deposited primer layer by reducing water transport across the film through cross-linking of the polymer mortar and improving

film adhesion to the steel substrate through silanization.

The nanobrick wall structure is formed by alternately depositing layers of cationic polyethylenimine (PEI) and anionic vermiculite (VMT) clay on steel. This PEI/VMT multilayer system has previously been shown to exhibit high gas barrier and some corrosion resistance stemming from the strong ionic bonding and the nanobrick wall structure that hinders corrosive species diffusion [19]. The high aspect ratio of VMT results in increased gas barrier properties over other clay alternatives, such as montmorillonite (MMT) or laponite (LAP) [20]. This thin film is cross-linked with glutaraldehyde (GA) to prevent water absorption and improve chemical, mechanical, and thermal stability [21, 22]. A silane pretreatment with aminoproplytriethoxysilane (APTES) promotes improved adhesion between the primer and steel, reducing delamination and microscale defects in the coating [23, 24]. This silanized and cross-linked nanobrick wall coating was tested as part of a multilayer system, utilizing a bisphenol-A based epoxy topcoat. By combining the already corrosion resistant epoxy with this nanocomposite primer, an improved and prolonged resistance to corrosive species is demonstrated. While cross-linking and silanization have been demonstrated to improve barrier properties, this study is the first time the methodologies have been combined to demonstrate improved corrosion resistance. This improvement demonstrates the viability of the functionalized nanobrick wall film to be used as an environmentally-benign primer layer in an multilayer insulating barrier coating for the protection of steel.

Experimental

Materials and substrates

Branched polyethylenimine (M_w = 25,000 g/mol), glutaraldehyde (25 wt.%), and (3-aminopropyl) triethoxysilane were purchased from Sigma-Aldrich (Milwaukee, WI). Microlite 963 + + vermiculite clay (7.8 wt.% in water) was purchased from Specialty Vermiculite Corp (Cambridge, MA) and diluted to a 1 wt.% suspension. Deionized (DI) water (with a resistivity equivalent to 18 MΩ) was used to prepare all solutions and rinses. All solutions were left at their intrinsic pH. 15.24 × 15.24 × 0.08 cm plates of A36

ground low-carbon steel was purchased from McMaster Carr (Aurora, OH) and cut to 2.54 × 2.54 cm coupons for coating. Metal substrates were cleaned by rinsing with DI water, methanol, and again DI water prior to bath sonicating in DI water and then isopropanol (IPA) for 2 min each, with IPA rinses between, and dried with filtered air. The steel was then immersed in a 1 M sodium hydroxide and 100 mM sodium nitrite solution overnight to passivate the surface for better adhesion prior to deposition. Bisphenol-A based epoxy (DER-671-X75) and a polyamide hardener (Versamide 140, Olin, Clayton, OH) were combined at 82.4 wt.% and 17.6 wt.%, respectively, and used as a topcoat.

Thin film preparation

Steel substrates were coated with bilayers of PEI/VMT using layer-by-layer (LbL) assembly, which was carried out with a home-built robotic system [25]. Films were assembled by first immersing the substrate into a 0.1 wt.% PEI solution for 1 min, followed by rinse and dry to remove any excess polymer. From there, the substrate was immersed in the 1 wt.% VMT solution for 1 min and then rinsed and dried again, which completes one bilayer (BL). This procedure, shown schematically in Fig. 1, was then repeated until the desired number of bilayers were deposited. Epoxy was coated using a birdbar with a 5 mil gap (127 μm) to generate a 2.5 mil (63.5 μm) thick coating once dry.

Cross-linking and silanization

Following LbL deposition, films were immersed in GA solutions of varying concentration to allow for cross-linking of the PEI layers, using immersion times of 1, 4, and 16 h. Additionally, the number of deposited BL (i.e., the thickness of the film) before cross-linking was evaluated by first comparing films cross-linked at 10, 15, and 20 BL. Films were then corrosion tested when cross-linked at 15 and 30 BL and compared to films cross-linked at only 30 BL. Prior to additional LbL deposition or testing, the sample was immersed in a 0.1 M sodium borohydride (NaBH4) solution (in ethanol) for one hour to reduce the Schiff base formed between GA and PEI [26]. Aminopropyltriethoxysilane was deposited on the surface of the steel prior to the LbL coating using vapor phase deposition, which took place under
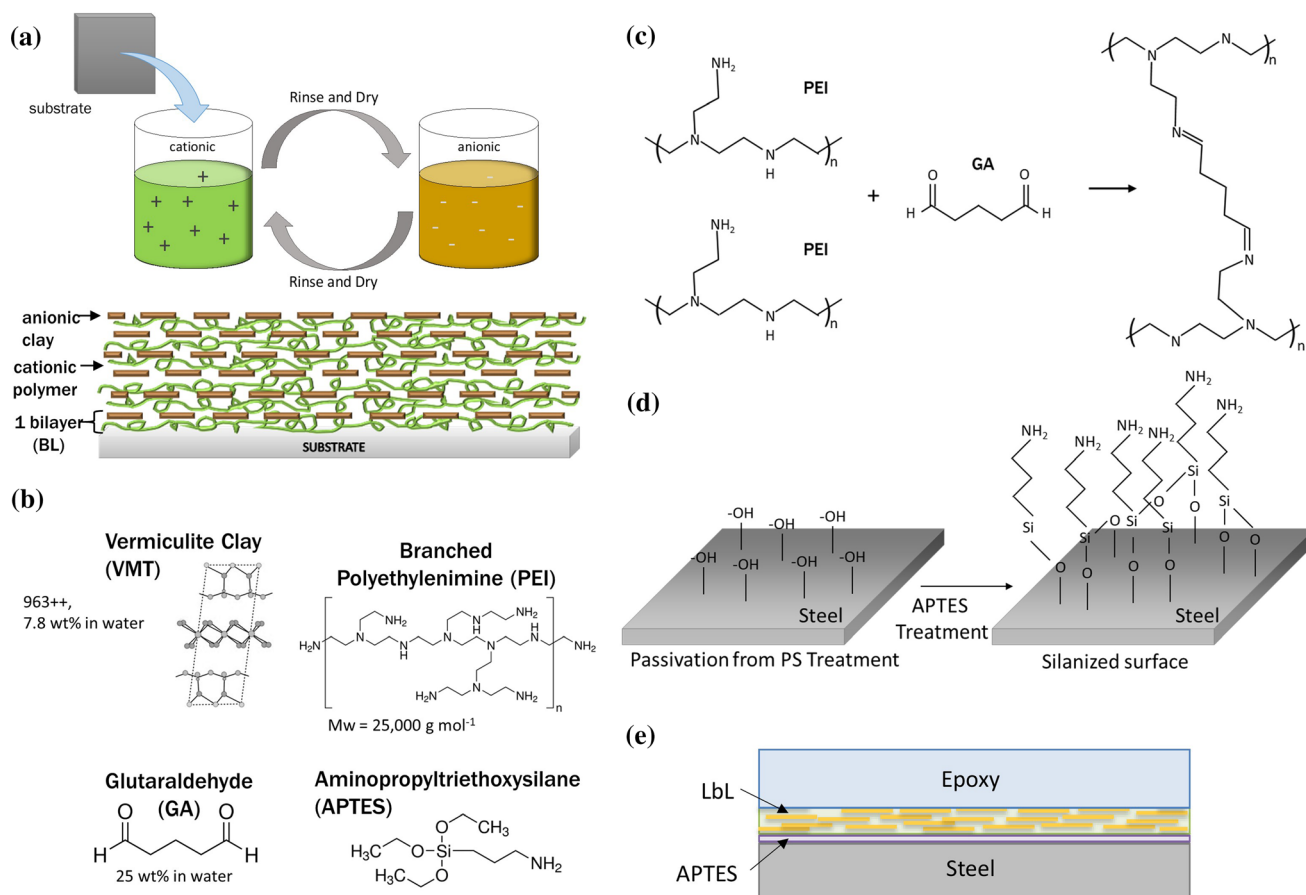
Figure 1 **(a)** Schematic of layer-by-layer (LbL) deposition process and corresponding nanobrick wall film and **(b)** materials used. Schematics of **(c)** PEI cross-linking using GA and **(d)** silanization of steel with APTES and **(e)** the final multilayer coating system.

vacuum. The substrate and 0.5 mL of APTES were placed in a vacuum desiccator overnight. LbL coating was done the following day after the sample was removed from vacuum. The cross-linking chemistry and silanization procedure are shown in Fig. 1.

Characterization

Corrosion testing was carried out by using a typical three electrode set up including the sample as the working electrode (with an exposed area of 1.766 cm^2), calomel saturated electrode as the reference and platinum mesh as the counter electrode. The experimental interfacial characterization included electrochemical impedance spectroscopy (EIS) (Gamry, Warminster, PA). During testing, films were exposed to 3.5 wt.% NaCl solution. Samples without an epoxy topcoat were tested for 24 h and compared to uncoated steel samples tested under the same conditions. Samples tested with an epoxy topcoat were examined over a 5 day period, with measurements

taken every hour for the first 24 h and then once a day for each subsequent day. Multilayer films were compared to an epoxy coated sample prepared without any pretreatments or LbL primer. Films were grown on polished silicon wafers (University Wafer, Boston, MA) for thickness and swelling measurements. A 5-min plasma cleaning treatment, using a PDC-32G plasma cleaner (Harrick Plasma, Ithaca, NY), was performed on silicon wafers prior to deposition. An Alpha-SE ellipsometer (J.A. Woollman Co., Inc., Lincoln, NE) was used to measure film swelling and a P-6 Stylus profilometer (KLA-Tencor, Milpitas, CA) was used to measure film thickness after intermittent cross-linking. For swelling measurements, the films were exposed to DI water for 15 min and thickness measurements taken prior to and after exposure. Adhesion testing was done using a crosshatch adhesion test, following ASTM D3359.

Results and discussion

Improved corrosion barrier through cross-linking

Nanobrick wall multilayer thin films are well known for their tremendous gas barrier behavior [17, 27]. The diffusion of molecules through the film is hindered by the high tortuosity created by the clay platelets. To further improve the film's resistance to diffusion, glutaraldehyde cross-linking of the amine groups in PEI is used to generate a polymeric network that reduces water uptake in the PEI/VMT film and availability of amine groups to stem chloride ion diffusion through the film. Unfortunately, the clay filler in the polymer composite film hinders effective cross-linking through the bulk of the film [28, 29]. To create a cohesive polymer network, optimal cross-linking conditions for the polymer–clay thin film are evaluated here using swelling measurements, where films with a greater extent of cross-linking display less swelling. Figure 2 shows the influence of immersion time, GA solution concentration, and film thickness (i.e., number of BL deposited) have on cross-linking. The extent of swelling is reduced in films cross-linked with higher GA concentration, extended exposure time, and lower thickness. Once 5% GA is reached, there does not appear to be greater cross-linking with greater concentration. These parameters likely allow more GA to diffuse into the nanobrick wall structure, creating a more dense polymer network. The denser network improves the moisture resistivity of the film, reducing overall swelling and susceptibility to aggressive ion transfer through the film.

Electrochemical impedance spectroscopy (EIS) testing was done on a reduced set of variables to demonstrate how cross-linking the polymeric mortar in the nanobrick wall film creates an improved corrosion barrier. To examine the influence of film thickness, deposition was done at two 15 BL intervals, with subsequent cross-linking after each, and compared with a 30 BL film cross-linked after only the final bilayer. Improved corrosion barrier can be seen in the increase of impedance values at low frequency, $|Z|_{0.1\ Hz}$. Values for each test are provided in Table 1. The films cross-linked at a greater GA concentration, and at both 15 and 30 BL, exhibit a higher $|Z|_{0.1\ Hz}$ value. These results further suggest that films exposed to GA at fewer BL (i.e., decreased thickness) have a greater extent of cross-linking and correspondingly improved corrosion resistance.

Following this established intermittent cross-linking procedure, a reduced set of GA concentrations were evaluated to determine the best concentration for promoting corrosion resistance. For this analysis, films were cross-linked with 2, 5, and 10 wt.% GA. Figure 3 shows the Nyquist and Bode plots for these tests. Each of the cross-linked films provides some level of corrosion protection, outperforming the uncross-linked 30 BL film. The film cross-linked with 5 wt.% GA has the best corrosion resistance. Cross-linking with 2 wt.% GA likely does not achieve the same level of networking, allowing for increased diffusion of corrosive species through the film. This can be seen in both the reduced $|Z|_{0.01\ Hz}$ value, compared to either the 5 wt.% or 10 wt.% cross-linked
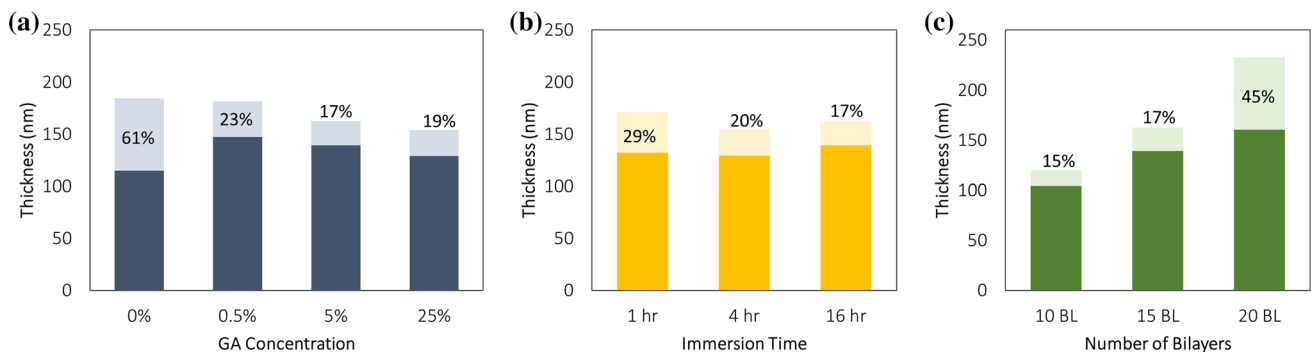

Figure 2 Swelling measurements for PEI/VMT multilayer films cross-linked at varying **(a)** GA concentration with cross-linking overnight on 15 BL, **(b)** cross-linking immersion time with 5% GA concentration on 15 BL, and **(c)** bilayers deposited before cross-linking with 5% GA overnight. The darker part of the bar is film thickness prior to testing and the lighter color is the thickness following exposure to water for 15 min.

Table 1 Impedance values for cross-linked films

GA Concentration (wt.%)	Cross-linked at 30 BL Resistivity $|Z|_{0.01\ Hz}$ ($\Omega \cdot cm^2$)	Cross-linked at 15 and 30 BL Resistivity $|Z|_{0.01\ Hz}$ ($\Omega \cdot cm^2$)
0%	2,925	–
0.5%	7,407	9,327
5%	9,197	19,006
25%	6,166	14,032

Figure 3 EIS **(a)** Nyquist and **(b)** Bode plots for 24 h of testing 30 BL PEI/VMT, cross-linked with various GA concentrations: 0 (red), 2 (yellow), 5 (purple), and 10% (green).
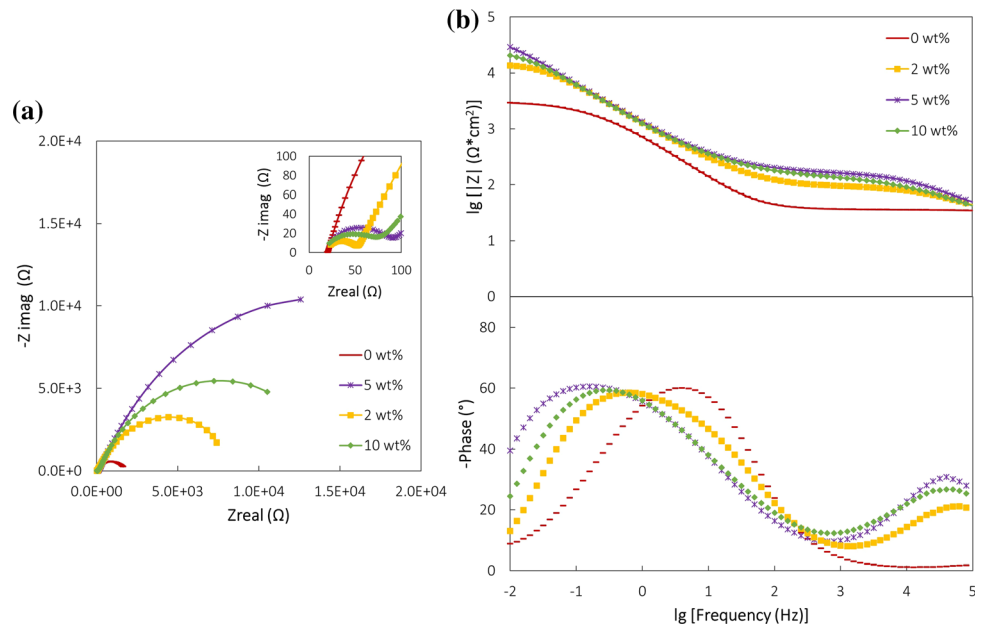
films, and a reduced magnitude observed in the Nyquist plot. Conversely, the exposure of the film to a greater concentration of GA (i.e., 10% or more) possibly results in plasticizing of the film due to excess unreacted small molecules present. It is also possible that the corrosive nature of GA, particularly at high concentration, initiates corrosion prior to testing, expediting failure of the film.
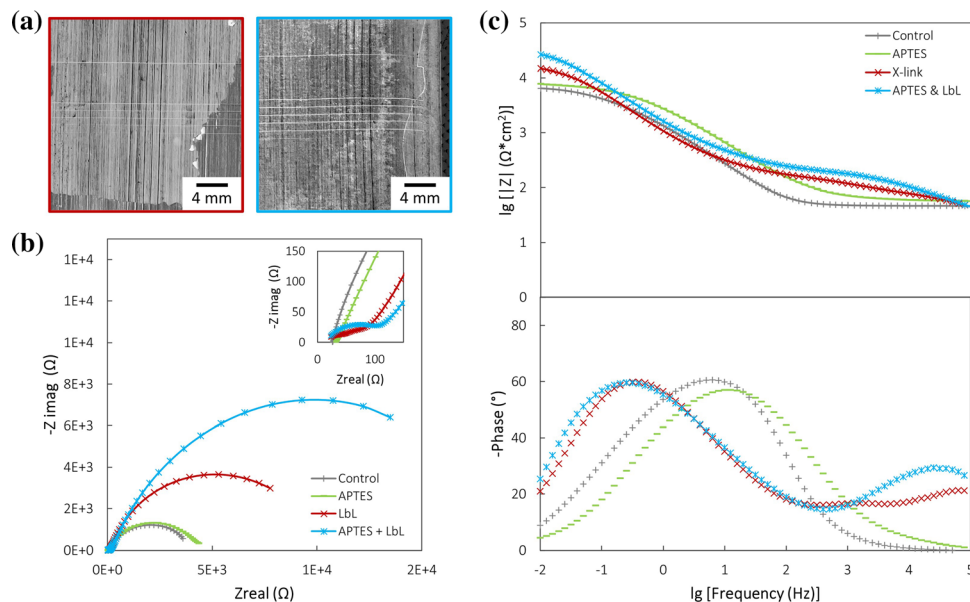
Silanization for adhesion

Corrosion resistance garnered by cross-linked nano-brick wall thin films is further improved with silane functionalization of the steel surface prior to film deposition. While the independent corrosion resistance achieved by a pretreatment coating is important, the primary role of this layer is to improve the adhesion between a topcoat and the underlying metal. Bonding of cationic PEI to steel is promoted by first exposing the metal to a 1 M sodium hydroxide

and 100 mM sodium nitrate solution to generate a hydroxide layer on the surface. As a result, the polymeric layer hydrogen bonds with the generated inorganic hydroxylated surface. While sufficient for promoting adhesion between PEI and steel during the deposition process, this pretreatment offers little adhesion once the film is dry. By introducing aminopropyltriethoxysilane, an organic surface is created that promotes improved hydrogen bonding. Vapor phase deposition of the APTES onto the surface of the metal allows for less variability in the formation of the Si-O-Si bonds between the silane and the metal [30, 31].

When PEI is deposited onto the APTES-treated steel, the PEI strongly bonds with the amine groups in the APTES chains through hydrogen bonding between the two organic layers. This superior adhesion is confirmed through the use of a crosshatch adhesion test, following ASTM standard D3359, shown in Fig. 4a. The film deposited on the steel

Figure 4 **(a)** Digital images of adhesion testing with (left) and without (right) APTES pretreatment, where the darker gray is the remaining coating following the test. **(b)** Nyquist plot after 24 h of EIS testing and **(c)** corresponding Bode impedance (top) and phase (bottom) plots.

without APTES has no apparent adhesion, with full delamination from the surface, while the film deposited following silanization exhibits improved adhesion. EIS testing demonstrates the extent to which this improved adhesion influences the corrosion resistance. Independently, the APTES offers no corrosion resistance, likely hydrolyzing and delaminating from the steel quickly upon exposure to the testing solution. Conversely, the benefits of the silanization between the film and substrate can be seen in the larger magnitude displayed in the Nyquist curve (Fig. 4b). Further, the impedance value, $|Z|_{0.01 \text{ Hz}}$, reported in Table 2, is greater and is indicative of improved corrosion barrier. As APTES adds no thickness to the overall system, the improved corrosion resistance can be attributed to the adhesion generated through better bonding.

Multilayer insulating system

The most successful corrosion resistant barrier coatings make use of multiple layers in tandem to protect a metal substrate. To demonstrate the viability of the silanized and cross-linked nanobrick wall thin film

for use as a primer layer in a multilayer system, an epoxy topcoat was applied and tested over 5 days. This is a corrosion resistant bisphenol-A based epoxy coating [32, 33]. A control of the epoxy coating alone is compared to epoxy paired with APTES, and a 30 BL PEI/VMT film, cross-linked at 15 and 30 BL with 5% GA, with and without silanization. Evaluation of the Bode plots show the contrast between the epoxy control and the system with the cross-linked and silanized nanobrick wall primer. While the neat epoxy system, shown in Fig. 5a, starts with the greatest $|Z|_{0.01 \text{ Hz}}$ value, the apparent corrosion resistance deteriorates over 5 days. Independently, the silanization and the cross-linking of the PEI/VMT film (Fig. 5b and c) do not perform well. The silanized epoxy starts out lower than the neat epoxy sample and deteriorates from there, demonstrating that APTES is not a good interface between the steel and epoxy topcoat. The nanobrick wall film also starts out poorly, but its reduction in performance over 5 days is less and seems stable after the first dip in performance. Only the cross-linked and silanized nanobrick wall film (Fig. 5d) exhibits sustained corrosion resistance over the five-day testing period.

Table 2 Thickness and impedance values due to APTES treatment

Sample	Thickness (nm)	Impedance $|Z|_{0.01 \text{ Hz}}$ ($\Omega*cm^2$)
Control Steel	–	6,438
APTES	1.3 ± 0.1	7,729
Nanobrick Wall	314.6 ± 9.7	19,006
APTES + Nanobrick Wall	315.0 ± 14.9	26,152
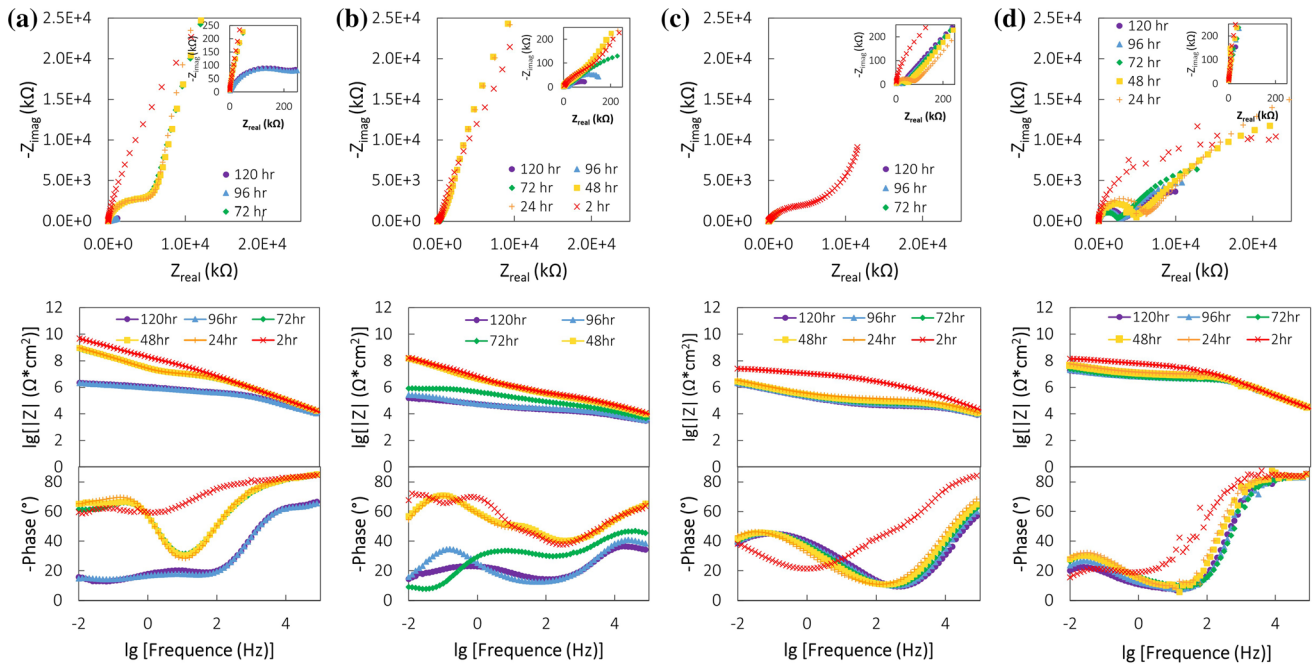
Figure 5 EIS Nyquist (top) and Bode (bottom) plots comparing films with an epoxy topcoat and pretreatment layer of **(a)** hydroxylated steel alone, **(b)** APTES-treated steel, **(c)** a 30 BL cross-linked (with 5% GA) PEI/VMT coating, and **(d)** the same nanobrick wall primer on APTES-treated steel.
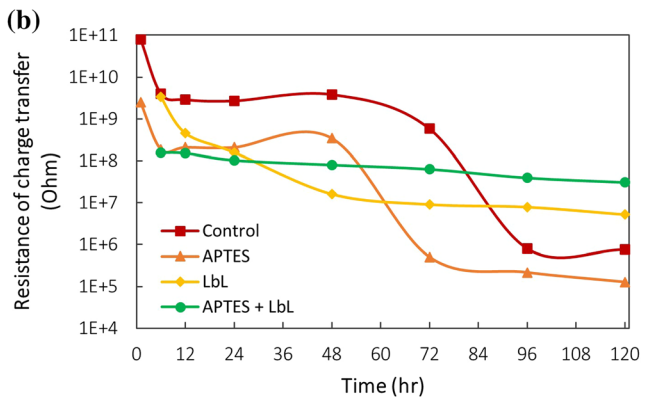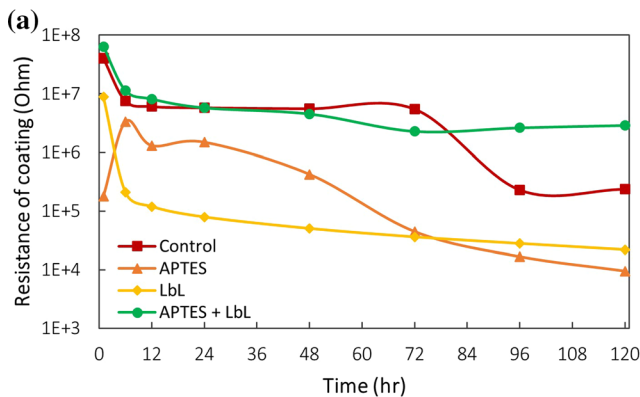
Figure 6 Equivalent circuit modeling of **(a)** resistivity and **(b)** charge transfer resistance of various systems with an epoxy top coat: control (red), APTES alone (orange), 30 BL PEI/VMT cross-linked (yellow), and the combination of APTES and the same cross-linked PEI/VMT (green).

Fitting these multilayer films to an equivalent circuit model provides insight into the overall interfacial characterization, including the corrosion resistance of each system. Figure 6a and b shows film resistivity and charge transfer resistance over the 5 days of testing, respectively. The full data set and equivalent circuit models for the fitting can be found in the Supplementary Information (Tables S1, S2, S3, and S4 and Figure S1(a)–(f)). The resistance of the coating is indicative of the overall barrier performance. The system performance is also evaluated with the charge

transfer resistance. Charge transfer occurs at the interface between the coating and the substrate as electrons enter the metal and metal ions diffuse out. Initially, APTES alone outperforms the LbL deposited coating, likely due to poor adhesion between PEI and the steel. The trend observed, particularly in the charge transfer resistance, is similar when comparing the APTES and control coating, indicative of the performance of the epoxy coating without the additional polymer nanocomposite primer. The APTES sample does not perform as well, which is possibly a

result of poor interfacial bonding between the silane and the epoxy. Additionally, an improvement in film resistance is temporarily observed in the APTES sample. As the water infiltrates the epoxy, but prior to the dissolution of the APTES layer, APTES may hydrolyze, briefly imparting greater interaction with the epoxy and increasing the overall resistance of the system. APTES alone does not show a robust corrosion barrier, so the overall barrier performance begins to degrade, ultimately having the least film and charge transfer resistivity of the tested samples. Most importantly, the fitting data confirms that the only film that performed well over all 5 days of testing was the combination of APTES, and cross-linked nanobrick wall film, with the epoxy topcoat (APTES + LbL). At the beginning of the test, the sample's film resistivity is equivalent to the independent epoxy system. As the test solution diffuses through the epoxy, and the neat epoxy film resistivity drops, the film resistivity of the sample paired with the silanized and cross-linked nanobrick wall film remains stable. Additionally, the prolonged resistance displayed by the silanized and cross-linked nanobrick wall film pretreatment to the charge transfer is accounted for by the improved adhesion between the PEI/VMT coating and the steel through APTES silanization.

Conclusions

The use of a layer-by-layer deposited nanobrick wall primer provides good corrosion protection to a steel substrate. Once silanized and cross-linked, the potential for these PEI/VMT coatings increases greatly, offering not only improved corrosion protection but also improved adhesion to the steel. These properties make them a good option as an alternative pretreatment layer for multilayer insulating coatings. The network generated by the cross-linked PEI promotes moisture resistance and a reduced vulnerability to aggressive ions permeating the coating. The APTES promotes improved adhesion that hinders delamination and reduces the available surface for corrosion induction. Combining the two methodologies with the nanobrick wall structure, which already hinders molecular diffusion through the tortuous path created by clay nanoplatelets, provides environmentally-benign corrosion protection.

Data availability

The data that support the finding of this study are available from the corresponding author upon request.

Declarations

Conflict of interest The authors declare no conflict of interest.

Supplementary Information: The online version contains supplementary material available at https://doi.org/10.1007/s10853-021-06706-3.

References

[1] Renner FU, Stierle A, Dosch H et al (2006) Initial corrosion observed on the atomic scale. Nature 439:707–710. https://doi.org/10.1038/nature04465

[2] Anticorrosive coatings: a review | SpringerLink. https://link.springer.com/article/https://doi.org/10.1007/s11998-008-9144-2. Accessed 11 Oct 2019

[3] Hou Y, Lei D, Li S et al (2016) Experimental investigation on corrosion effect on mechanical properties of buried metal pipes. Int J Corros 2016:5808372. https://doi.org/10.1155/2016/5808372

[4] Revie RW, Uhlig HH (2008) Corrosion and corrosion control: an introduction to corrosion science and engineering, 4th edn. Wiley-Interscience, Hoboken, N.J.

[5] Geary W, Hobbs J (2013) Catastrophic failure of a carbon steel storage tank due to internal corrosion. Case Stud Eng Fail Anal 1:257–264. https://doi.org/10.1016/j.csefa.2013.09.002

[6] Stierle A (2008) Tracking corrosion cracking. Science 321:349–350. https://doi.org/10.1126/science.1160939

[7] Zarras P, Stenger-Smith JD (2014) 1–Corrosion processes and strategies for prevention: an introduction. In: Makhlouf ASH (ed) Handbook of Smart Coatings for Materials Protection. Woodhead Publishing, pp 3–28

[8] Andreeva DV, Skorb EV (2014) Multi-layer smart coatings for corrosion protection of aluminium alloys and steel. In:

Handbook of Smart Coatings for Materials Protection. Elsevier, pp 307–327

[9] al-Swaidani AA (2017) Modified zinc phosphate coatings: a promising approach to enhance the anti-corrosion properties of reinforcing steel. MOJ Civ Eng 3, https://doi.org/10.1540/mojce.2017.03.00083

[10] Narayanan S (2005) Surface pretreatment by phosphate conversion coatings–a review. Rev Adv Mater Sci 9:130–177

[11] Ucaroglu S, Talinli İ (2012) Recovery and safer disposal of phosphate coating sludge by solidification/stabilization. J Environ Manage 105:131–137. https://doi.org/10.1016/j.jenvman.2012.03.029

[12] Qian Y, Li Y, Jungwirth S et al (2015) The application of anti-corrosion coating for preserving the value of equipment asset in chloride-laden environments: a review. Int J Electrochem Sci 10:26

[13] Shchukin DG, Zheludkevich M, Yasakau K et al (2006) Layer-by-layer assembled nanocontainers for self-healing corrosion protection. Adv Mater 18:1672–1678. https://doi.org/10.1002/adma.200502053

[14] Sinha Ray S, Okamoto M (2003) Polymer/layered silicate nanocomposites: a review from preparation to processing. Prog Polym Sci 28:1539–1641. https://doi.org/10.1016/j.progpolymsci.2003.08.002

[15] Suarez-Martinez PC, Robinson J, An H et al (2018) Polymer-clay nanocomposite coatings as efficient, environment-friendly surface pretreatments for aluminum alloy 2024–T3. Electrochim Acta 260:73–81. https://doi.org/10.1016/j.electacta.2017.11.046

[16] Yeh J-M, Liou S-J, Lai C-Y et al (2001) Enhancement of corrosion protection effect in polyaniline via the formation of polyaniline−clay nanocomposite materials. Chem Mater 13:1131–1136. https://doi.org/10.1021/cm000938r

[17] Priolo MA, Holder KM, Greenlee SM, Grunlan JC (2012) Transparency, gas barrier, and moisture resistance of large-aspect-ratio vermiculite nanobrick wall thin films. ACS Appl Mater Interfaces 4:5529–5533. https://doi.org/10.1021/am3014289

[18] Qin S, Cubides Y, Lazar S et al (2018) Ultrathin transparent nanobrick wall anticorrosion coatings. ACS Appl Nano Mater 1:5516–5523. https://doi.org/10.1021/acsanm.8b01032

[19] Percival SJ, Melia MA, Alexander CL et al (2020) Nanoscale thin film corrosion barriers enabled by multilayer polymer clay nanocomposites. Surf Coat Technol 383:125228. https://doi.org/10.1016/j.surfcoat.2019.125228

[20] Xiang F, Tzeng P, Sawyer JS et al (2014) Improving the gas barrier property of clay-polymer multilayer thin films using shorter deposition times. ACS Appl Mater Interfaces 6:6040–6048. https://doi.org/10.1021/am403445z

[21] Maitra J, Shukla (2014) Hydrogels, Cross linking, Gel, Polymer. Am J Polym Sci 7

[22] Lindén JB, Larsson M, Kaur S et al (2016) Glutaraldehyde-crosslinking for improved copper absorption selectivity and chemical stability of polyethyleneimine coatings. J Appl Polym Sci. https://doi.org/10.1002/app.43954

[23] Liu Y, Cao H-J, Yu Y, Chen S (2015) Corrosion protection of silane coatings modified by carbon nanotubes on stainless steel. Int J Electrochem Sci 10:3497–3509

[24] Howarter JA, Youngblood JP (2006) Optimization of silica silanization by 3-aminopropyltriethoxysilane. Langmuir 22:11142–11147. https://doi.org/10.1021/la061240g

[25] Jang WS, Grunlan JC (2005) Robotic dipping system for layer-by-layer assembly of multi-functional thin films. Rev Sci Instrum 76:103904

[26] Yang Y-H, Bolling L, HaileC Grunlan MJ (2012) Improving oxygen barrier and reducing moisture sensitivity of weak polyelectrolyte multilayer thin films with crosslinking. RSC Adv 2:12355–12363. https://doi.org/10.1039/C2RA21845C

[27] Hagen DA, Saucier L, Grunlan JC (2014) Controlling effective aspect ratio and packing of clay with ph for improved gas barrier in nanobrick wall thin films. ACS Appl Mater Interfaces 6:22914–22919. https://doi.org/10.1021/am507603z

[28] Karabanova L, Sergeeva L, Boiteux G (2001) Filler effect on formation and properties of reinforced interpenetrating polymer networks. Compos Interfaces 8:207–219. https://doi.org/10.1163/15685540152594677

[29] Ruijgrok JM, De Wijn JR, Boon ME (1994) Optimizing glutaraldehyde crosslinking of collagen: effects of time, temperature and concentration as measured by shrinkage temperature. J Mater Sci Mater Med 5:80–87. https://doi.org/10.1007/BF00121695

[30] Yuan X, Wolf N, Mayer D et al (2019) Vapor-phase deposition and electronic characterization of 3-aminopropyltriethoxysilane self-assembled monolayers on silicon dioxide. Langmuir 35:8183–8190. https://doi.org/10.1021/acs.langmuir.8b03832

[31] Zhang F, Sautter K, Larsen AM et al (2010) Chemical vapor deposition of three aminosilanes on silicon dioxide: surface characterization, stability, effects of silane concentration, and cyanine dye adsorption. Langmuir 26:14648–14654. https://doi.org/10.1021/la102447y

[32] de Miranda MIG, Tomedi C, Bica CID, Samios D (1997) A d.s.c. kinetic study on the effect of filler concentration on crosslinking of diglycidylether of bisphenol-A with 4,4′-diaminodiphenylmethane. Polymer 38:1017–1020. https://doi.org/10.1016/S0032-3861(96)00601-5

[33] Vermeirssen ELM, Dietschweiler C, Werner I, Burkhardt M (2017) Corrosion protection products as a source of bisphenol A and toxicity to the aquatic environment. Water Res 123:586–593. https://doi.org/10.1016/j.watres.2017.07.006

Publisher's Note Springer Nature remains neutral with regard to jurisdictional claims in published maps and institutional affiliations.